Available online at www.sciencedirect.com

ScienceDirect

International Journal of Solids and Structures 44 (2007) 8627–8647

INTERNATIONAL JOURNAL OF SOLIDS AND STRUCTURES

www.elsevier.com/locate/ijsolstr

Characterization and development of an evolutionary yield function for the superconducting niobium sheet

Amir Zamiri, Farhang Pourboghrat *

Mechanical Engineering Department, Michigan State University, East Lansing, MI 48824, United States

Received 19 December 2006; received in revised form 2 May 2007; accepted 26 June 2007
Available online 4 July 2007

Abstract

Superconducting radio frequency (SRF) niobium cavities are widely used in high-energy physics to accelerate particle beams in particle accelerators. The performance of SRF cavities is affected by the microstructure and purity of the niobium sheet, surface quality, geometry, etc. Following optimum strain paths in the forming of these cavities can significantly control these parameters. To select these strain paths, however, information about the mechanical behavior, microstructure, and formability of the niobium sheet is required. Due to the lack of information, first an extensive experimental study was carried out to characterize the formability of the niobium sheet, followed by examining the suitability of Hill's anisotropic yield function to model its plastic behavior. Results from this study showed that, due to intrinsic behavior, it is necessary to evolve the anisotropic coefficients of Hill's yield function in order to properly model the plastic behavior of the niobium sheet. The accuracy of the newly developed evolutionary yield function was verified by applying it to the modeling of the hydrostatic bulging of the niobium sheet.

Keywords: Evolutionary yield function; High purity niobium; Texture; Sheet metal forming

1. Introduction

The superconducting accelerator niobium cavities, shown in Fig. 1, are traditionally fabricated by deep drawing of subcomponents, which are later joined by electron beam welding. High purity niobium sheet is the favorite material for the fabrication of these cavities. The knowledge of the mechanical properties of the niobium sheet plays a significant role in the fabrication and treatment of these cavities. Most laboratories working on superconducting accelerator technology have strict requirements for the niobium material that they use, and have developed a quality assurance (QA) strategy for this purpose. Nevertheless, the quality control tests that they perform are limited in scope. But recently, due to the need for more powerful accelerators, new fabrication techniques for making seamless cavities have been considered. The idea of manufacturing seamless cavities would have the following benefits:

* Corresponding author. Tel.: +1 517 353 0819; fax: +1 517 353 1750.
E-mail address: pourbogh@egr.msu.edu (F. Pourboghrat).

0020-7683/$ - see front matter
doi:10.1016/j.ijsolstr.2007.06.025

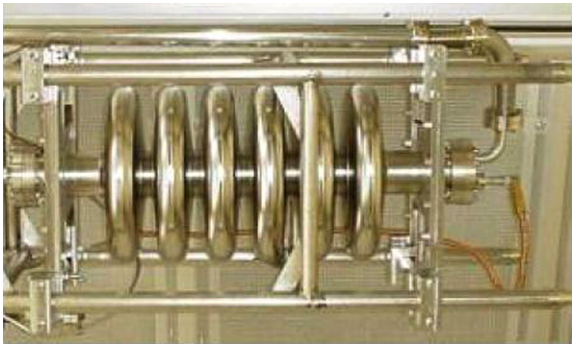

Fig. 1. A six cell superconducting accelerator niobium cavity (Courtesy of National Superconducting Cyclotron Laboratory at Michigan State University).

- Elimination of electron beam welds.
- Improvement of mechanical and physical properties of the cavities.
- Reduction of manufacturing costs.
- Facilitating mass production.

Several attempts has been made by Kneisel and Palmieri (1999), Palmieri (1999), and Singer et al. (2001a,b) to fabricate seamless cavities by using techniques such as tube hydroforming, explosive forming, or spinning of deep drawn or spun tubes and more recently combination of swaging and hydroforming of high purity niobium tubes.

It was shown by Pagani et al. (2001) that the most important issue to be considered in the manufacturing of these cavities is the optimum design of its geometry; such as the cell length, iris radius, sidewall inclination and position, cell radius, etc. Therefore, the forming processes must be carefully selected in order to produce the desired geometry after deformation. For this purpose, understanding the material behavior and developing accurate constitutive and mathematical models are important. Kneisel and Palmieri (1999) reported observing non-uniformity in the hydroformed highly pure niobium cavities, which they thought was related to the non-uniformity of the structure of the niobium tube.

Several investigators, e.g. Nakamachi and Xie (2003), Asensio et al. (2001) have shown that for good formability, the material must have the following properties:

- High r_m value (mean normal anisotropy coefficients).
- High n value (work hardening exponent).
- Low Δr value (planar anisotropy coefficient or earring parameter, which is responsible for cross section geometry and thickness variation).

All the above parameters can be measured from simple tensile tests at different directions, compared with rolling direction. The ductility of the material also can be precisely determined using these tests. Asensio et al. (2001) reported that texture has a strong influence on r_m value and Δr in cold formed and annealed metallic sheets, however, n value is primarily influenced by the chemical composition and the presence of second-phase particles, and only secondarily by the grain size. More recently, Zamiri et al. (2006) provided an overview of the mechanical properties and microstructure of superconducting niobium sheet.

Anisotropy has a significant effect on the strain distribution in a metallic alloy sheet forming. The anisotropy of a metal in a sheet metal forming process is a combination of the initial anisotropy of the sheet before forming, which is related to the initial microstructure and texture of the sheet metal, and the deformation-induced anisotropy, which is due to the microstructure and texture evolution of the sheet metal during forming process. The initial anisotropy leads to a symmetry with orthotropic properties in a sheet metal while the deformation-induced anisotropy can destroy this symmetry and make the modeling of the plastic anisotropy

very complex in a forming process. Therefore, for practical purpose, it is assumed that the deformation-induced anisotropy is small and negligible. Several anisotropic yield functions for modeling the plastic deformation of metals have been proposed based on this assumption. For example, One may see the quadratic yield function proposed by Hill (1948), non-quadratic functions developed by Hill (1979, 1990), Hershey (1954), Hosford (1972), Bassani (1977), Gotoh (1977), Logan and Hosford (1980), Budianski (1984), Barlat and Lian (1989), Barlat et al. (1991, 1993, 1997, 2003), Yoon et al. (2003).

Up to now, there have not been any published results about the forming properties of the high purity niobium sheet. In this paper we will attempt to evaluate its forming properties by means of experimental and numerical studies. The layout of this paper is as follows. In Section 2, the experimental work to characterize the mechanical properties of the high purity niobium sheet will be described. In Section 3, an evolutionary yield function for the high purity niobium sheet will be proposed. Sections 4–6 will describe the incremental formulation and the simulation results of the application of the evolutionary yield function to the modeling of the hydrostatic bulging of the niobium sheet. Finally, Section 7 will discuss the texture and its effect on the forming behavior of the high purity niobium sheet.

2. Experimental characterization

The material used in the experiments was a 2 mm thick high purity superconducting niobium sheet manufactured by Tokyo Denkai Company. The chemical composition of the superconducting niobium sheet is shown in Table 1. To evaluate the formability and the anisotropy of the rolled niobium sheet, uniaxial tensile tests in different directions, compared to the rolling direction, were carried out. The tensile tests were conducted following the ASTM E517 standard. To carefully capture the anisotropic plastic ratio or the r-value ($=d\varepsilon_{width}/d\varepsilon_{thickness}$) of the niobium sheet during the uniaxial tensile test, transverse and axial extensometers were used and also the elastic part of strain was calculated and subtracted from the total strain to maintain the volume constancy. To evaluate the texture of the sheet, the OIM (Orientation Imaging Microscopy) measurements on the initial sheet and the uniaxially deformed sheet were carried out. The orientation distribution functions (ODFs) were then captured from the OIM measurements.

2.1. Mechanical properties and formability of the niobium sheet

2.1.1. Yield stress variation

In general, the inelastic deformation of BCC crystalline materials is strongly rate and temperature dependent, e.g., see Read-Hill and Kaufman (1994). There are two explanations for this behavior; one explanation is that the rate controlling mechanism is associated with the Peierls-Nabarro potential barriers to dislocation motion. The other rate controlling mechanism is the thermal activation of mobile dislocations past interstitial solute atoms. In the high purity superconducting niobium sheet four kinds of interstitial atoms have been observed which are C, N, H, and O. The rate controlling mechanism of plastic deformation in niobium is considered to be due to the movement of screw dislocations by thermally activated formation of kink pairs over a Peierls potential, e.g., see Nemat-Nasser and Guo (2000). On the other hand, the deformation of niobium is affected by the interaction between the dislocations and interstitial and substitutional atoms. The experimental stress–strain curves obtained from the uniaxial tensile tests performed at various directions in the plane of the sheet are shown in Fig. 2. It can be seen that with the exception of the rolling direction (0-direction), the stress–strain curves in other directions are similar. The variation of the yield stress in the plane of the sheet, measured using the 0.2% offset strain, is shown in Fig. 3 (experiment). Again, it can be seen that the maximum difference

Table 1
Chemical composition of superconducting niobium sheet

Element	Ta	W	Ti	Fe	Si	Mo	Ni	Zr	Hf	O	N	C	H
Composition (wt%)	0.024	<0.002	<0.001	<0.001	<0.001	<0.001	<0.001	<0.001	<0.001	<0.001	<0.001	<0.001	<0.0002

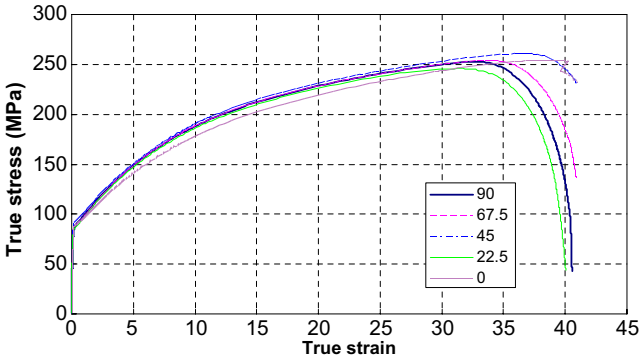

Fig. 2. True stress–strain curves obtained from the uniaxial tensile test performed along different directions with respect to the rolling direction.

in the magnitude of the measured yield stress in the plane of the sheet is less than 3.5 MPa. Table 2 shows the parameters of the Holloman equation ($\bar{\sigma} = K\bar{\varepsilon}^n$) fitted to the uniaxial stress–strain curves in different directions for the superconducting niobium sheet.

2.1.2. Yield function

In this paper, the following non-quadratic yield function proposed by Logan and Hosford (1980) for anisotropic materials is considered:

$$af(\sigma_{ij}) \equiv F|\sigma_y - \sigma_z|^a + G|\sigma_z - \sigma_x|^a + H|\sigma_x - \sigma_y|^a + 2L|\tau_{yz}|^a + 2M|\tau_{xz}|^a + 2N|\tau_{xy}|^a \quad (1)$$

where the exponent "a" is an even, integer number (e.g., $a = 6$ for BCC and $a = 8$ for FCC metals), and parameters F, G, H, L, M and N are the anisotropy coefficients. It should be noted that by setting the exponent $a = 2$, Hill's (1948) quadratic, anisotropic yield function would be recovered.

In sheet metal forming processes, deformation takes place under the plane stress condition. Choosing the axes of the anisotropy such that the x-axis lies in the rolling direction, y-axis in the transverse direction, and z-axis normal to the plane of the sheet metal, then, for any stress state in the plane of the sheet the non-quadratic yield function, Eq. (1), reduces to

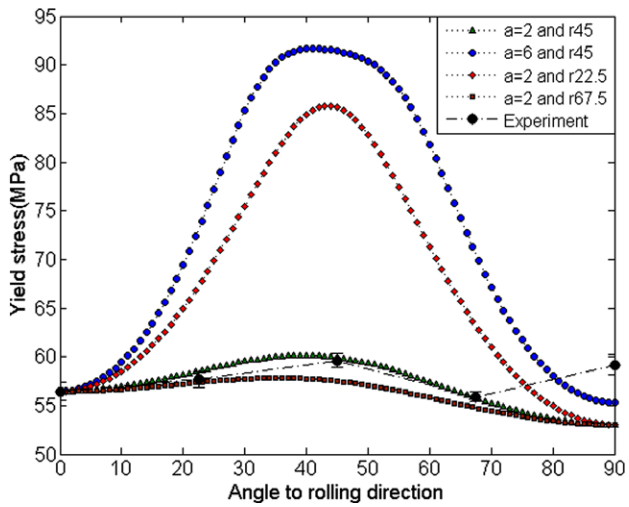

Fig. 3. Measured versus predicted variation of the yield stress (using 0.2% offset method) as a function of the angle to the rolling direction for the niobium sheet. Predicted values are based on various a- and r-values.

Table 2
Parameters of Hollomon equation for superconducting niobium

Direction	K (MPa)	n
0°	351.25	0.2942
22.5°	361.58	0.2954
45°	368.15	0.2941
67.5°	374.09	0.3059
90°	360.14	0.2894

$$af(\sigma_{ij}) = F|\sigma_y|^a + G|\sigma_x|^a + H|\sigma_x - \sigma_y|^a + 2N|\tau_{xy}|^a = X^a(G+H) \tag{2}$$

where in Eq. (2) it is assumed that yielding, under any stress combination, occurs according to the uniaxial tensile flow stress in the rolling direction, X. For a tensile test carried out in the plane of the sheet and in an arbitrary direction θ ($0 \leqslant \theta \leqslant 90$) to the rolling direction:

$$\sigma_x = \sigma_f \cos^2, \quad \theta\sigma_y = \sigma_f \sin^2\theta, \quad \tau_{xy} = \sigma_f \sin\theta\cos\theta \tag{3}$$

where σ_f is the tensile flow stress in θ-direction. By substituting the above expressions into Eq. (2), σ_f can be expressed as a function of the flow stress in the rolling direction, X, and the anisotropy coefficients:

$$\sigma_f(\theta) = \frac{X\cdot(G+H)^{1/a}}{[F\sin^{2a}\theta + G\cos^{2a}\theta + H|\cos^a 2\theta| + 2N|\sin^a\theta\cos^a\theta|]^{1/a}} \tag{4}$$

Also, using the normality rule (i.e., $\dot{\varepsilon} = \dot{\lambda}\partial f/\partial\sigma$), the r-value ($=\mathrm{d}\varepsilon_{\mathrm{width}}/\mathrm{d}\varepsilon_{\mathrm{thickness}}$) can be calculated as a function of θ-direction:

$$r_\theta = -\frac{G|\cos^2\theta|^{a-1}\cdot\sin^2\theta + F|\sin^2\theta|^{a-1}\cdot\cos^2\theta - H|\cos 2\theta|^{a-1}\cdot\cos 2\theta - 2N|\sin\theta\cos\theta|^{a-1}\cdot\sin\theta\cos\theta}{G|\cos^2\theta|^{a-1} + F|\sin^2\theta|^{a-1}} \tag{5}$$

From Eq. (5), by setting $\theta = 0$ and $\theta = 90°$ we can recover $r_0 = \frac{H}{G}$ and $r_{90} = \frac{H}{F}$ respectively. By choosing:

$$F = r_0, \quad G = r_{90}, \quad H = r_0.r_{90} \tag{6a}$$

and by substituting these relationships into Eq. (5), the following expression can be obtained for the anisotropy parameter N:

$$N = \frac{1}{2}\left[\frac{r_\theta(r_{90}\cos^m\theta + r_0\sin^m\theta) + (r_{90}\cos^m\theta\sin^2\theta + r_0\sin^m\theta\cos^2\theta - r_0 r_{90}\cos^a 2\theta)}{\sin^a\theta\cos^a\theta}\right] \tag{6b}$$

where $m = 2(a-1)$. For the quadratic case ($a = 2$), Eq. (6b) simplifies to

$$N = \frac{1}{2}\left[\frac{r_\theta(r_0\sin^2\theta + r_{90}\cos^2\theta) - r_0 r_{90}}{\sin^2\theta\cos^2\theta} + r_0 + r_{90} + 4r_0 r_{90}\right] \tag{6c}$$

The anisotropy coefficients F, G, H and N therefore can be calculated using only three r-values measured between 0 and 90° to the rolling direction. Table 3 shows the r-values measured at 18% plastic strain, according to the M517-ASTM standard, for the high purity niobium sheet.

The calculated values of F, G, H and N at 18% plastic strain can be found in Fig. 9. Once the four anisotropy coefficients were calculated, they were substituted into Eq. (4) to calculate the variation of the yield stress at different orientation to the rolling direction. To calculate the coefficient N, using Eq. (6b), r_θ was selected in

Table 3
The r-values for the high purity niobium sheet measured at 18% plastic strain (M517-ASTM Standard)

r_0	$r_{22.5}$	r_{45}	$r_{67.5}$	r_{90}
2.25	1.15	1.37	1.52	1.57

such a way to minimize the difference between the calculated yield stress variation and the experimental curve. Fig. 3 shows the variation of the yield stress calculated with the yield function exponents $a = 2$ and $a = 6$ using the r_θ values at $\theta = 22.5°$, $\theta = 45°$ and $\theta = 67.5°$. It can be seen from Fig. 3 that the yield stress variation predicted with $a = 2$ and r_θ at $\theta = 45°$ gives the best overall prediction for the yield stress variation in the plane of the superconducting niobium sheet. However, it should be noted that none of the models were able to accurately capture the yield strength of the niobium in the transverse direction (i.e., 90°). This is primarily caused by having only four parameters in the Hill's yield function to capture a larger number of experimentally measured r-values and yield strengths. To eliminate this problem, it will be necessary to use a yield function with more parameters. Based on the results in Fig. 3 it was decided, for the remainder of the paper, to only use the Hill's quadratic yield function (i.e., $a = 2$).

2.1.3. The r-value variation and normal anisotropy of the high purity niobium sheet

The r-value, which is also known as the plastic anisotropy ratio, is used to evaluate the formability of a sheet metal. Its variation in the plane of the sheet provides a good criterion for evaluating the geometrical variation in a deep drawn part. Usually the r-value of a material remains constant at large plastic strains. Fig. 4, however, shows that the r-value of the niobium sheet is very sensitive to the plastic strain and changes as strain increases and its variation is different in different directions. Therefore, using the r-value or the mean r-value to evaluate the plastic behavior of the high purity niobium sheet will not be sufficient. To investigate this issue further, the Hill's quadratic yield function ($a = 2$) was used to predict the r-value variation for the high purity niobium.

Starting with Eq. (5) and setting $a = 2$, the following expression for r_θ can be obtained:

$$r_\theta = \frac{H + (2N - F - G - 4H)\sin^2\theta\cos^2\theta}{F\sin^2\theta + G\cos^2\theta} \tag{6}$$

Eq. (6) contains four anisotropy parameters, F, G, H and N, which are determined using three r_θ values, as discussed in the previous section. According to the ASTM standard, r_θ must be evaluated at the strain from which the r-value remains constant. For BCC materials (e.g., steel, niobium, etc.), it is typical to evaluate the r-value in the range of 15–20% strain. For the niobium sheet, r_θ-values were evaluated along 0, 45° and 90° at 18% plastic strain. Using these three r_θ-values, F, G, H and N were calculated using Eqs. (6a) and (6c). Then, by substituting these four parameters into Eq. (6), r_θ-values were predicted based on the Hill's quadratic yield function. Fig. 5 shows a comparison of these predicted r_θ-values versus measured ones at three different plastic strains of 5%, 18%, and 30%. It can be seen that except for the case of 18% plastic strain, the predicted r_θ-values do not match the experimental data very well. These figures show that at 5% plastic strain, the predicted r_θ-values underestimate the experimental r_θ-values, while at 30% plastic strain they overestimate them. Therefore,

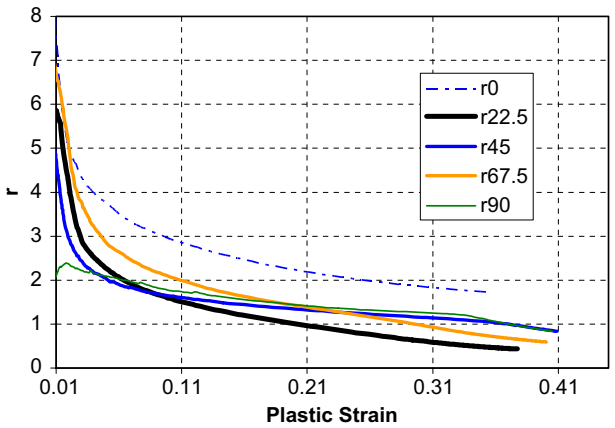

Fig. 4. Variation of the r-value with the plastic strain in different directions, compared to the rolling direction.

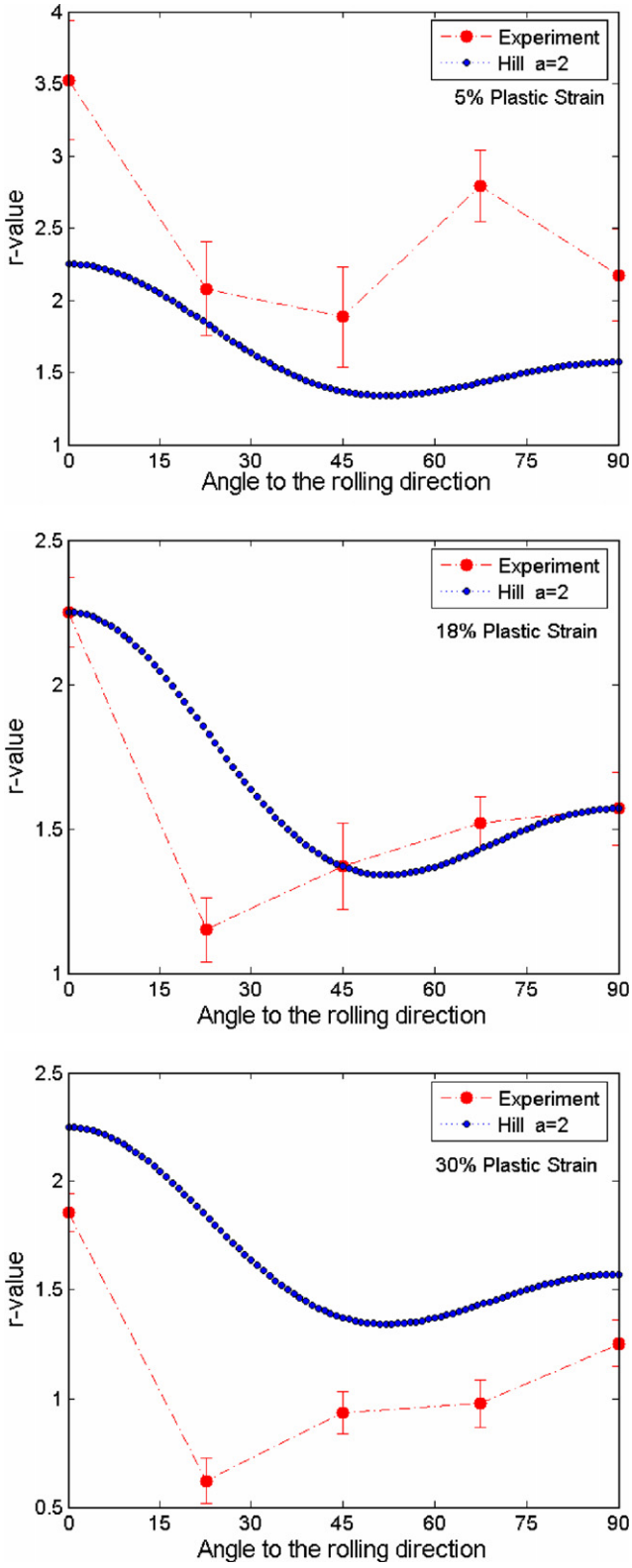

Fig. 5. A comparison of predicted r_θ-values against measured ones at three different plastic strain levels of 5%, 18%, and 30%. Predicted values are based on using quadratic Hill's yield function ($a = 2$) with constant anisotropic coefficients.

it can be concluded that for high purity niobium sheet, it is important to include in the material model the evolution of the r_θ-values with respect to the plastic strain.

2.1.4. Method of calculating the average r-value using experimental data

The average r-value and the planar anisotropy of the sheet are two important parameters to be considered when evaluating deep drawability and geometrical variation of the part. To calculate the average r-value, first the variation of the r-value as a function of the orientation, θ, in the plane of the sheet at a fixed strain will be considered, as follows:

$$r_\varepsilon(\theta) = \sum_{i=0}^{n} b_i \cos^i \theta, \quad \theta : \left[0, \frac{\pi}{2}\right] \text{ and } \varepsilon : [0, \varepsilon_n] \tag{7}$$

where ε_n is the maximum strain up to which the r-value is considered. Using Eq. (7), the average r-value can then be calculated as

$$\bar{r}_\varepsilon = \frac{2}{\pi} \int_0^{\frac{\pi}{2}} \sum_{i=0}^{n} b_i \cos^i \theta \, \mathrm{d}\theta \tag{8}$$

As can be seen from Fig. 4, the r-value for the high purity niobium sheet is very sensitive to the plastic strain. Therefore, another expression would be needed to account for this variation. Piehler (1967) has shown that the ideal r-value for BCC materials cannot be higher than 3. However, it can be seen from Fig. 4 that some of the r-values are much larger than 3, which is caused by the difficulty in accurately measuring this parameter at small strains. Therefore, to avoid introducing error in the calculation of the r-values, the following equation was used to account for the variation of the r-value with respect to the plastic strain at a fixed direction, θ:

$$r_\theta(\varepsilon) = \begin{cases} \sum_{i=0}^{m} c_i \varepsilon^i & \text{if } \varepsilon \geqslant \varepsilon_0 \\ \sum_{i=0}^{m} c_i \varepsilon_0^i & \text{if } \varepsilon \leqslant \varepsilon_0 \end{cases} \quad \text{and} \quad \varepsilon : [0, \varepsilon_n] \tag{9}$$

Or,

$$r_\theta(\varepsilon) = H\left(\sum_{i=0}^{m}(c_i\varepsilon_0^i - c_i\varepsilon^i)\right)\sum_{i=0}^{m} c_i\varepsilon_0^i + H\left(\sum_{i=0}^{m}(c_i\varepsilon^i - c_i\varepsilon_0^i)\right)\sum_{i=0}^{m} c_i\varepsilon^i \tag{10}$$

where $H(x)$ is Heaviside step function, with following properties: $H(x) = 1$ when $x > 0$, $H(x) = 0$ when $x < 0$, and $H(x) = 0.5$ when $x = 0$ and ε_0 is the minimum strain that gives reasonable r-values.

The average r-value at a given direction can then be calculated from Eq. (10) as

$$\bar{r}_\theta = \frac{1}{\varepsilon_n}\int_0^{\varepsilon_n} r_\theta \, \mathrm{d}\varepsilon = \frac{1}{\varepsilon_n}\left[\sum_{i=0}^{m} c_i\varepsilon_0^i \cdot \varepsilon_0 + \sum_{i=0}^{m} \frac{c_i}{i+1}(\varepsilon_n^{i+1} - \varepsilon_0^{i+1})\right] \tag{11}$$

The first five columns in Table 4 show the average r-values for the niobium sheet calculated from Eq. (11).

Combining Eqs. (7) and (10) yields the following expression for the variation of the r-value with respect to both plastic strain and θ-direction:

$$r(\varepsilon,\theta) = H\left(\sum_{i=0}^{m}(c_i(\theta)\varepsilon_0^i - c_i(\theta)\varepsilon^i)\right)\sum_{i=0}^{m} c_i(\theta)\varepsilon_0^i + H\left(\sum_{i=0}^{m}(c_i(\theta)\varepsilon^i - c_i(\theta)\varepsilon_0^i)\right)\sum_{i=0}^{m} c_i(\theta)\varepsilon^i \tag{12}$$

Table 4
Average r-values and Δr of highly pure niobium sheets

$\bar{r}_0$	$\bar{r}_{22.5}$	$\bar{r}_{45}$	$\bar{r}_{67.5}$	$\bar{r}_{90}$	$\bar{\bar{r}}(\bar{r}_m)$	$\Delta\bar{r}$
2.58	1.28	1.37	1.78	1.64	1.61	0.65

The mean r-value for the entire range of plastic strains and directions in the plane of the sheet is then:

$$\bar{\bar{r}} = \frac{2}{\pi\varepsilon_n}\int_0^{\frac{\pi}{2}}\int_0^{\varepsilon_n}\left[H\left(\sum_{i=0}^{m}(c_i(\theta)\varepsilon_0^i - c_i(\theta)\varepsilon^i)\right)\sum_{i=0}^{m}c_i(\theta)\varepsilon_0^i + H\left(\sum_{i=0}^{m}(c_i(\theta)\varepsilon^i - c_i(\theta)\varepsilon_0^i)\right)\sum_{i=0}^{m}c_i(\theta)\varepsilon^i\right]\mathrm{d}\varepsilon\,\mathrm{d}\theta \tag{13}$$

To obtain the r-value for the high purity niobium sheet, the variation of the r-value as a function of the plastic strain and direction was obtained by curve fitting Eq. (12) to the experimental data. Table 5, shows the coefficients of Eq. (10) for the high purity niobium sheet obtained by curve fitting the expression to the experimental data in five directions and using $m = 4$. To avoid any error associated with the unreliability of the r-values at small strains, curve fitting to the experimental data was performed at strains between 10% and 30%. Using Eq. (13), the mean r-value for the niobium sheet was computed to be $\bar{\bar{r}}(\bar{r}_m) = 1.61$, as shown in the sixth column of Table 4.

2.1.5. Planar anisotropy of the high purity niobium sheet

Fig. 5 shows the in-plane variation of the r-value with respect to the rolling direction. As will be discussed later in this paper, the large variation of the r-value with strain corresponds to the large variation in the texture of the niobium sheet during the forming process. It is well known that the cross section and thickness of a deep drawn part made with a material with high planar anisotropy will not be uniform and symmetric. Therefore, it can be expected that the geometry of the superconducting accelerator cavity will not be uniform either if formed with the niobium sheet. The planar anisotropy at a plastic strain can be defined as

$$\Delta r_\varepsilon = \bar{r}_{\max}|_\varepsilon - \bar{r}_{\min}|_\varepsilon$$

And at any strain:

$$\frac{\partial r_\varepsilon}{\partial\theta} = \frac{\partial}{\partial\theta}\left[\sum_{i=0}^{n} b_i\cos^i\theta\right] = 0 \tag{14}$$

$$r_{\text{extremum}}|_\varepsilon = \sum_{i=0}^{n} b_i\cos^i\theta_j$$

where θ_j are roots of Eq. (14).

And in general:

$$\Delta\bar{r} = \bar{\bar{r}}_{\max} - \bar{\bar{r}}_{\min} \tag{15}$$

The average planar anisotropy of the high purity niobium sheet calculated by Eq. (15) is shown to be $\Delta\bar{r} = 0.65$ in Table 4.

Fig. 6 shows the variation of Δr with respect to the plastic strain using Eqs. (10) and (11). This figure shows two discontinuities associated with the change in the number of extremum points. At strains smaller than 20%, the niobium sheet shows two maximums and two minimums for the variation of the r-value as a function of θ (Fig. 13). At strains between 20% and 25% it shows one minimum at 25° and two maximums; one very sharp at 0° and one very smooth at 90°. After 25%, it shows three maximums at 0°, 45°, and 90° and two minimums at 25° and 70°. Therefore, superconducting niobium sheet shows three different behaviors during the plastic deformation. These behaviors can be related to the existence of unstable components in the initial texture

Table 5
The coefficients of Eq. (10) for five directions obtained by curve fitting ($m = 4$)

Coefficient	C_0	C_1	C_2	C_3	C_4
r_0	4.325	−18.678	57.067	−98.746	70.972
$r_{22.5}$	2.840	−18.751	79.912	−199.750	198.678
r_{45}	2.432	−13.957	67.657	−172.400	155.240
$r_{67.5}$	4.030	−31.822	161.510	−415.970	393.750
r_{90}	2.778	−14.849	60.977	−109.880	50.617

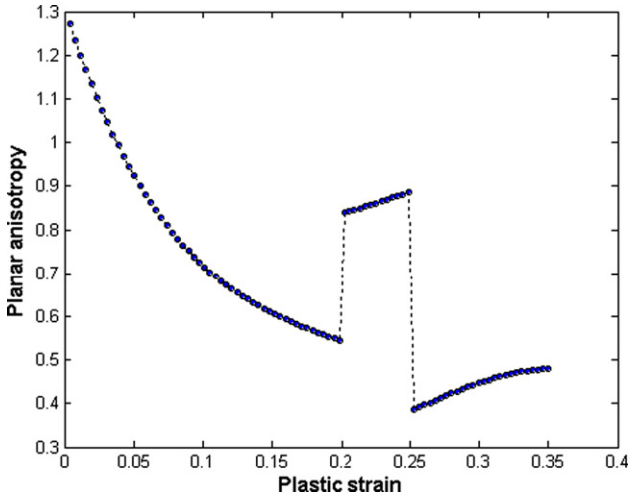

Fig. 6. Variation of the planar anisotropy with plastic strain.

of the material, which are unstable with respect to the uniaxial tension performed during the measurement of the r-values. Also Fig. 6 shows a decrease in the planar anisotropy of the niobium sheet with respect to the plastic strain. Using Eqs. (13) and (15), the total planar anisotropy of $\Delta\bar{r} = 0.65$ for the high purity niobium sheet was obtained.

3. An evolutionary yield function for the niobium sheet

As shown above, the plastic behavior of niobium sheet is complicated. Its r-value is sensitive to the plastic strain and direction. Therefore, in developing a yield function for niobium sheet one needs to take into account the variations of the r-values. Furthermore, the yield function should have enough parameters to accurately predict the forming properties of the high purity niobium sheet. In this study, Hill's yield function was used for this purpose; however, an ongoing effort is underway to develop a yield function based on Barlat's yield functions (1997, 2003, and 2004), which have more parameters. In general, for the high purity niobium sheet we will need to evolve the anisotropy parameters of the yield function using Eq. (12). In other words, we will need to update the values of the anisotropy parameters of the yield function at every deformation increment, as a function of strain. For example, for the yield function in Eq. (1), we will need to calculate $F(\varepsilon)$, $G(\varepsilon)$, $H(\varepsilon)$, and $N(\varepsilon)$ using Eq. (10). Fig. 7 shows the calculated values of F, G, H, and N as a function of plastic strain using Eq. (1), $a = 2$, and the values of r at 0°, 45°, and 90° computed using the data given in Table 5. Fig. 8 shows a comparison between the variations of the r-values obtained from the experiment with those predicted by Hill's yield function using the evolved anisotropic coefficients. In this case Hill's yield function provides a much better prediction for both low and high plastic strains.

Fig. 9 shows the percent error in predicted r-values with respect to the experimental data versus plastic strain using Hill's quadratic yield function with evolving and constant coefficients. The percent error was calculated using the experimental and predicted r-values at 0°, 22.5°, 45°, 67.5°, and 90°. As can be seen, the yield function with evolving coefficients (evolutionary yield function) gives a better prediction as compared with the yield function with constant coefficients (static yield function). It should be mentioned that by using a yield function with higher number of anisotropy coefficients, such as Barlat, 2003 , the magnitude of the percent error could be drastically reduced.

Fig. 10 shows the change in the shape of the Hill's yield function with plastic strain using evolving coefficients. The shape of the yield function is similar to a highly anisotropic material at lower plastic strains (e.g., 5%), but becomes more like an isotropic material as strain increases to 35%. Another interesting point to note about the behavior of an evolutionary yield function is that the direction of the normal to the yield surface (As seen from Fig. 10) at a particular stress condition also changes with plastic strain.

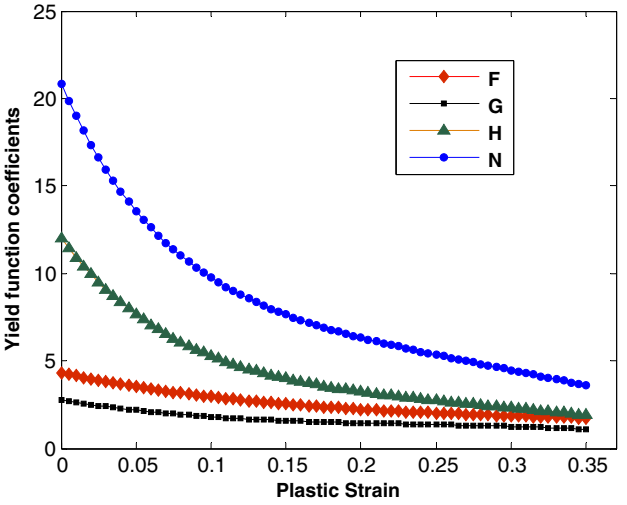

Fig. 7. Variation of the anisotropy coefficients of Hill's quadratic yield function as a function of plastic strain.

4. A stress integration algorithm for the plastic behavior of superconducting niobium sheet

Assuming that the flow stress along the rolling direction is X:

$$(X(\bar{\varepsilon}^p))^a \cdot [G(\bar{\varepsilon}^p) + H(\bar{\varepsilon}^p)] = 1$$

Substituting the above expression into Eq. (2) will result in the following yield function:

$$f = \left\{ \frac{F(\bar{\varepsilon}^p)}{G(\bar{\varepsilon}^p) + H(\bar{\varepsilon}^p)} |\sigma_y|^a + \frac{G(\bar{\varepsilon}^p)}{G(\bar{\varepsilon}^p) + H(\bar{\varepsilon}^p)} |\sigma_x|^a + \frac{H(\bar{\varepsilon}^p)}{G(\bar{\varepsilon}^p) + H(\bar{\varepsilon}^p)} |\sigma_x - \sigma_y|^a + \frac{2N(\bar{\varepsilon}^p)}{G(\bar{\varepsilon}^p) + H(\bar{\varepsilon}^p)} |\sigma_{xy}|^a \right\}^{\frac{1}{a}} - X(\bar{\varepsilon}^p) \tag{16}$$

It is assumed that the flow stress X changes according to a power-law form:

$$X(\bar{\varepsilon}^p) = K(\bar{\varepsilon}^p + \varepsilon_\circ)^n \tag{17}$$

Assuming the associate flow rule, the normality rule can be given as

$$\dot{\boldsymbol{\varepsilon}}^p = \dot{\lambda} \frac{\partial f}{\partial \boldsymbol{\sigma}} \tag{18}$$

Based on the Kohn–Tucker formulation for the optimality condition:

$$\dot{\lambda} f \leqslant 0$$

where

$$\dot{\bar{\varepsilon}}^p = \dot{\lambda}$$

Then the current rate of stress can be calculated as

$$\dot{\boldsymbol{\sigma}} = \mathbf{C} : (\dot{\boldsymbol{\varepsilon}}_t - \dot{\boldsymbol{\varepsilon}}_t^p) = \mathbf{C} : \dot{\boldsymbol{\varepsilon}}_t - \dot{\lambda} \mathbf{C} : \left. \frac{\partial f}{\partial \boldsymbol{\sigma}} \right|_t = \dot{\boldsymbol{\sigma}}_t - \dot{\lambda} \mathbf{C} : \left. \frac{\partial f}{\partial \boldsymbol{\sigma}} \right|_t \tag{19}$$

where the index t indicates the value at the beginning of the increment. Considering an incremental formulation, then based on the backward-Euler return method we will have

$$\mathbf{r} = \boldsymbol{\sigma} - \left(\boldsymbol{\sigma}_t - \lambda \mathbf{C} : \left. \frac{\partial f}{\partial \boldsymbol{\sigma}} \right|_c \right) \tag{20}$$

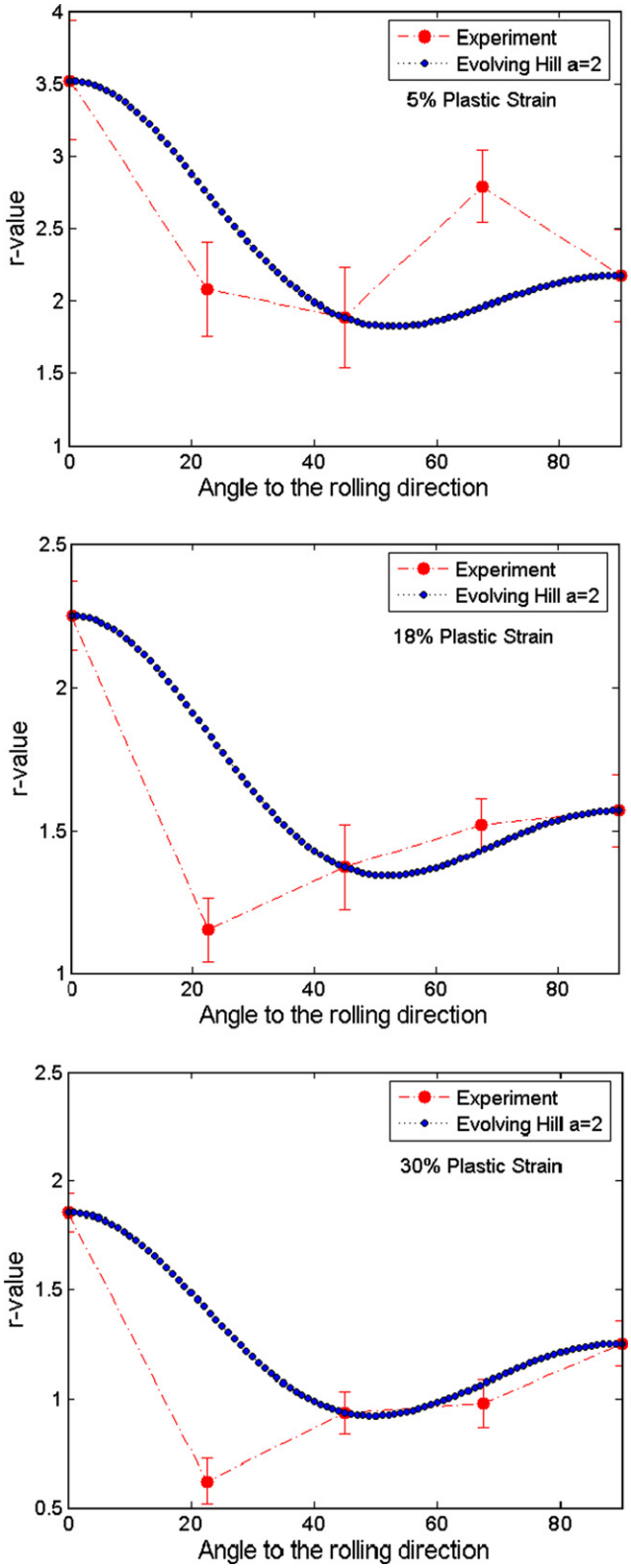

Fig. 8. Variations of the *r*-values using Hill's quadratic yield function with evolving coefficients as compared with experimental data.

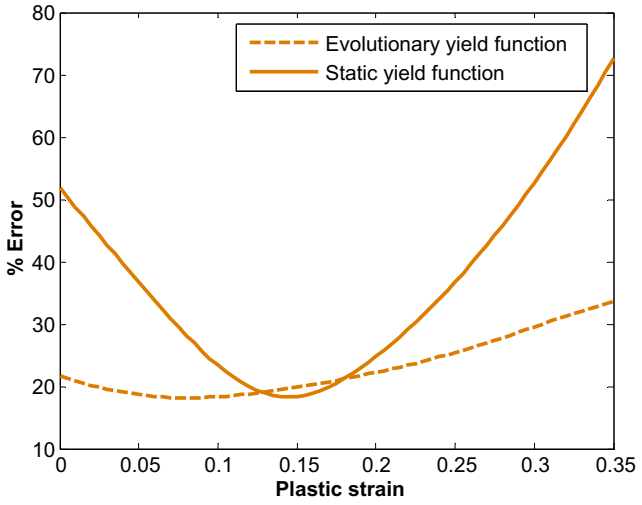

Fig. 9. The percent error in predicted r-values (with respect to the experimental data) versus plastic strain using Hill's quadratic yield function with evolving coefficients (evolutionary yield function) and with constant coefficients (static yield function).

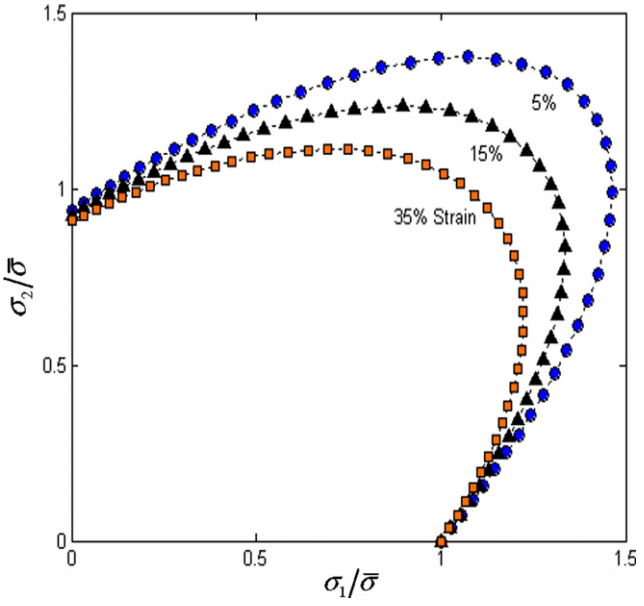

Fig. 10. Shape change of the Hill's yield function with plastic strain in niobium sheets.

where $\mathbf{r}$ is the stress residual and index c indicates the value at the end of the increment. A Taylor's expansion of the above equation produces a new residual:

$$\mathbf{r} = \mathbf{r}_\circ + \Delta\boldsymbol{\sigma} + \lambda\mathbf{C} : \frac{\partial}{\partial\boldsymbol{\sigma}}\left(\frac{\partial f}{\partial\boldsymbol{\sigma}}\right)\bigg|_c \Delta\boldsymbol{\sigma} + \lambda\mathbf{C} : \frac{\partial}{\partial\mathbf{Q}}\left(\frac{\partial f}{\partial\boldsymbol{\sigma}}\right)\cdot\Delta\mathbf{Q} + \Delta\lambda\mathbf{C} : \frac{\partial f}{\partial\boldsymbol{\sigma}}\bigg|_c = 0 \tag{21}$$

where $\mathbf{Q}$ is a matrix containing the values of F, H, G, and N.

Also, a Taylor's expansion of the yield function gives:

$$f = f_\circ + \frac{\partial f}{\partial\boldsymbol{\sigma}}\bigg|_c : \Delta\boldsymbol{\sigma} + \frac{\partial f}{\partial\mathbf{Q}}\cdot\Delta\mathbf{Q} + \frac{\partial f}{\partial\bar{\varepsilon}^p}\bigg|_c \Delta\bar{\varepsilon}^p = 0 \tag{22}$$

These two equations can be solved simultaneously to obtain the change in the Lagrange multiplier:

$$\Delta\lambda = \frac{f_\circ - \frac{\partial f}{\partial \boldsymbol{\sigma}}\Big|_c : \mathbf{M}^{-1}\mathbf{r}_\circ}{\frac{\partial f}{\partial \boldsymbol{\sigma}}\Big|_c : \mathbf{M}^{-1}\mathbf{C} : \frac{\partial f}{\partial \boldsymbol{\sigma}}\Big|_c + \frac{\partial f}{\partial \boldsymbol{\sigma}}\Big|_c : \mathbf{M}^{-1}\left(\lambda\mathbf{C} : \frac{\partial}{\partial \mathbf{Q}}\left(\frac{\partial f}{\partial \boldsymbol{\sigma}}\right)\Big|_c \frac{\partial \mathbf{Q}}{\partial \bar{\varepsilon}^p} + \frac{\partial f}{\partial \mathbf{Q}}\frac{\partial \mathbf{Q}}{\partial \bar{\varepsilon}^p}\right) + \frac{\partial f}{\partial \boldsymbol{\sigma}}\Big|_c : \mathbf{M}^{-1}\frac{\partial f}{\partial \bar{\varepsilon}^p}\Big|_c} \tag{23}$$

where

$$\mathbf{M} = \mathbf{I} + \lambda\mathbf{C} : \frac{\partial}{\partial \boldsymbol{\sigma}}\left(\frac{\partial f}{\partial \boldsymbol{\sigma}}\right)\Big|_c \tag{24}$$

For an implicit formulation, the algorithmic elastoplastic tangent moduli must be calculated. The incremental updating of stresses and plastic strains can be expressed as

$$\boldsymbol{\sigma}_{n+1} = \mathbf{C} : (\boldsymbol{\varepsilon}_{n+1} - \boldsymbol{\varepsilon}^p_{n+1}) \tag{25}$$

$$\boldsymbol{\varepsilon}^p_{n+1} = \boldsymbol{\varepsilon}^p_n + \lambda_{n+1}\frac{\partial f(\boldsymbol{\sigma}_{n+1}, \mathbf{Q}_{n+1}, \bar{\varepsilon}^p_{n+1})}{\partial \boldsymbol{\sigma}} \tag{26}$$

The differential form of the above equations is expressed as

$$\mathrm{d}\boldsymbol{\sigma}_{n+1} = \mathbf{C} : (\mathrm{d}\boldsymbol{\varepsilon}_{n+1} - \mathrm{d}\boldsymbol{\varepsilon}^p_{n+1}) \tag{27}$$

$$\begin{aligned}\mathrm{d}\boldsymbol{\varepsilon}^p_{n+1} &= \lambda_{n+1}\frac{\partial^2 f(\boldsymbol{\sigma}_{n+1}, \mathbf{Q}_{n+1}, \bar{\varepsilon}^p_{n+1})}{\partial \boldsymbol{\sigma}^2} \\ &\quad : \mathrm{d}\boldsymbol{\sigma}_{n+1} + \lambda_{n+1}\frac{\partial}{\partial \mathbf{Q}}\left(\frac{\partial f(\boldsymbol{\sigma}_{n+1}, \mathbf{Q}_{n+1}, \bar{\varepsilon}^p_{n+1})}{\partial \boldsymbol{\sigma}}\right)\mathrm{d}\mathbf{Q}_{n+1} + \frac{\partial f(\boldsymbol{\sigma}_{n+1}, \mathbf{Q}_{n+1}, \bar{\varepsilon}^p_{n+1})}{\partial \boldsymbol{\sigma}}\mathrm{d}\lambda_{n+1}\end{aligned} \tag{28}$$

And for the yield function coefficients we have

$$\mathrm{d}\mathbf{Q}_{n+1} = \frac{\partial \mathbf{Q}(\bar{\varepsilon}^p_{n+1})}{\partial \bar{\varepsilon}^p}\mathrm{d}\bar{\varepsilon}^p_{n+1} = -\frac{\partial \mathbf{Q}(\bar{\varepsilon}^p_{n+1})}{\partial \bar{\varepsilon}^p}\mathrm{d}\lambda_{n+1} \tag{29}$$

Combining Eqs. (27)–(29):

$$\mathrm{d}\boldsymbol{\sigma}_{n+1} = \boldsymbol{\Xi}_{n+1} : \left[\mathrm{d}\boldsymbol{\varepsilon}_{n+1} + \left(\lambda_{n+1}\frac{\partial}{\partial \mathbf{Q}}\left(\frac{\partial f(\boldsymbol{\sigma}_{n+1}, \mathbf{Q}_{n+1}, \bar{\varepsilon}^p_{n+1})}{\partial \boldsymbol{\sigma}}\right)\frac{\partial \mathbf{Q}}{\partial \bar{\varepsilon}^p_{n+1}} - \frac{\partial f(\boldsymbol{\sigma}_{n+1}, \mathbf{Q}_{n+1}, \bar{\varepsilon}^p_{n+1})}{\partial \boldsymbol{\sigma}}\right)\mathrm{d}\lambda_{n+1}\right] \tag{30}$$

where

$$\boldsymbol{\Xi}_{n+1} = \left[\mathbf{C}^{-1} + \lambda_{n+1}\frac{\partial^2 f(\boldsymbol{\sigma}_{n+1}, \mathbf{Q}_{n+1}, \bar{\varepsilon}^p_{n+1})}{\partial \boldsymbol{\sigma}^2}\right]^{-1} \tag{31}$$

In Eq. (30) $\mathrm{d}\lambda$ is unknown, but can be calculated using the consistency condition $\lambda f = 0$ due to the plastic condition $\lambda > 0$. Therefore, $f(\boldsymbol{\sigma}, \mathbf{Q}, \bar{\varepsilon}^p) = 0$ and differentiation of discrete consistency condition yields:

$$\frac{\partial f(\boldsymbol{\sigma}_{n+1}, \mathbf{Q}_{n+1}, \bar{\varepsilon}^p_{n+1})}{\partial \boldsymbol{\sigma}} : \mathrm{d}\boldsymbol{\sigma}_{n+1} + \frac{\partial f(\boldsymbol{\sigma}_{n+1}, \mathbf{Q}_{n+1}, \bar{\varepsilon}^p_{n+1})}{\partial \mathbf{Q}}\mathrm{d}\mathbf{Q}_{n+1} + \frac{\partial f(\boldsymbol{\sigma}_{n+1}, \mathbf{Q}_{n+1}, \bar{\varepsilon}^p_{n+1})}{\partial \bar{\varepsilon}^p}\mathrm{d}\bar{\varepsilon}^p_{n+1} = 0 \tag{32}$$

Substituting for $\mathrm{d}\mathbf{Q}$ and $\mathrm{d}\boldsymbol{\sigma}$ from Eqs. (29) and (30) into Eq. (32) gives

$$\mathrm{d}\lambda_{n+1} = \frac{\frac{\partial f}{\partial \boldsymbol{\sigma}}\Big|_{n+1} : \boldsymbol{\Xi}_{n+1} : \mathrm{d}\boldsymbol{\varepsilon}_{n+1}}{\frac{\partial f}{\partial \boldsymbol{\sigma}}\Big|_{n+1} : \boldsymbol{\Xi}_{n+1} : \left(\frac{\partial f}{\partial \boldsymbol{\sigma}}\Big|_{n+1} - \lambda_{n+1}\frac{\partial}{\partial \mathbf{Q}}\left(\frac{\partial f}{\partial \boldsymbol{\sigma}}\right)_{n+1} \cdot \frac{\partial \mathbf{Q}}{\partial \bar{\varepsilon}^p_{n+1}}\right) + \frac{\partial f}{\partial \mathbf{Q}}\Big|_{n+1} \cdot \frac{\partial \mathbf{Q}}{\partial \bar{\varepsilon}^p}\Big|_{n+1} + \frac{\partial f}{\partial \bar{\varepsilon}^p}\Big|_{n+1}} \tag{33}$$

By substituting for $\mathrm{d}\lambda$ from Eq. (33) into Eq. (30), the elastoplastic tangent moduli can be obtained:

$$\mathbf{C}^{ep} = \frac{\mathrm{d}\boldsymbol{\sigma}}{\mathrm{d}\boldsymbol{\varepsilon}}\Big|_{n+1} = \boldsymbol{\Xi}_{n+1} + r^{-1}\mathbf{T}_{n+1} \otimes \mathbf{S}_{n+1} \tag{34}$$

where

$$\mathbf{T}_{n+1} = \mathbf{\Xi}_{n+1} : \left(\lambda_{n+1} \frac{\partial}{\partial \mathbf{Q}} \left(\frac{\partial f(\boldsymbol{\sigma}_{n+1}, \mathbf{Q}_{n+1}, \bar{\varepsilon}^p_{n+1})}{\partial \boldsymbol{\sigma}} \right) \frac{\partial \mathbf{Q}(\bar{\varepsilon}^p_{n+1})}{\partial \bar{\varepsilon}^p} - \frac{\partial f(\boldsymbol{\sigma}_{n+1}, \mathbf{Q}_{n+1}, \bar{\varepsilon}^p_{n+1})}{\partial \boldsymbol{\sigma}} \right)$$

$$\mathbf{S}_{n+1} = \mathbf{\Xi}_{n+1} : \frac{\partial f(\boldsymbol{\sigma}_{n+1}, \mathbf{Q}_{n+1}, \bar{\varepsilon}^p_{n+1})}{\partial \boldsymbol{\sigma}}$$

$$r = \frac{\partial f(\boldsymbol{\sigma}_{n+1}, \mathbf{Q}_{n+1}, \bar{\varepsilon}^p_{n+1})}{\partial \boldsymbol{\sigma}} : \mathbf{\Xi}_{n+1} : \left(\frac{\partial f(\boldsymbol{\sigma}_{n+1}, \mathbf{Q}_{n+1}, \bar{\varepsilon}^p_{n+1})}{\partial \boldsymbol{\sigma}} - \lambda_{n+1} \frac{\partial}{\partial \mathbf{Q}} \left(\frac{\partial f(\boldsymbol{\sigma}_{n+1}, \mathbf{Q}_{n+1}, \bar{\varepsilon}^p_{n+1})}{\partial \boldsymbol{\sigma}} \right) \cdot \frac{\partial \mathbf{Q}(\bar{\varepsilon}^p_{n+1})}{\partial \bar{\varepsilon}^p_{n+1}} \right) + \frac{\partial f(\boldsymbol{\sigma}_{n+1}, \mathbf{Q}_{n+1}, \bar{\varepsilon}^p_{n+1})}{\partial \mathbf{Q}} \cdot \frac{\partial \mathbf{Q}(\bar{\varepsilon}^p_{n+1})}{\partial \bar{\varepsilon}^p} + \frac{\partial f(\boldsymbol{\sigma}_{n+1}, \mathbf{Q}_{n+1}, \bar{\varepsilon}^p_{n+1})}{\partial \bar{\varepsilon}^p}$$

5. Numerical algorithm

Based on the above equations the following implicit integration algorithm can be developed to model the plastic deformation of the niobium sheet:

1. Input the values of $\Delta\boldsymbol{\varepsilon}_n, \bar{\varepsilon}^p_n, \boldsymbol{\sigma}_n$ at the beginning of the increment n
2. Assuming elastic solution, update the stresses at the end of the increment (Elastic predictor):

$$\boldsymbol{\sigma}_{n+1} = \boldsymbol{\sigma}_n + \mathbf{C} : \Delta\boldsymbol{\varepsilon}_\mathbf{n}$$
$$\bar{\varepsilon}^p_{n+1} = \bar{\varepsilon}^p_n$$
$$\mathbf{Q}_{n+1} = \mathbf{Q}(\bar{\varepsilon}^p_{n+1})$$

3. If $f(\boldsymbol{\sigma}_{n+1}, \mathbf{Q}_{n+1}, \bar{\varepsilon}^p_{n+1}) \leqslant 0$, we have an Elastic solution.

$$\left.\frac{\mathrm{d}\boldsymbol{\sigma}}{\mathrm{d}\boldsymbol{\varepsilon}}\right|_{n+1} = \mathbf{C}, \text{ Exit}$$

Endif

4. Plastic corrector:

$$k = 0$$
$$\lambda^{(k)}_{n+1} = 0$$
$$\Delta\lambda^{(k)}_{n+1} = 0$$

5. Update hardening, yield coefficients, and stresses:

$$\bar{\varepsilon}^{p(k)}_{n+1} = \bar{\varepsilon}^p_{n+1} + \lambda^{(k)}_{n+1}$$
$$X(\bar{\varepsilon}^{p(k)}_{n+1}) = K(\bar{\varepsilon}^{p(k)}_{n+1} + \varepsilon_\circ)^n$$
$$\mathbf{Q}^{(k)}_{n+1} = \mathbf{Q}(\bar{\varepsilon}^{p(k)}_{n+1})$$
$$\boldsymbol{\sigma}^k_{n+1} = \boldsymbol{\sigma}_{n+1} - \lambda^{(k)}_{n+1} \mathbf{C} : \frac{\partial f(\boldsymbol{\sigma}_{n+1}, \mathbf{Q}_{n+1})}{\partial \boldsymbol{\sigma}}$$

6. If $f(\sigma^{(k)}_{n+1}, \mathbf{Q}^{(k)}_{n+1} \bar{\varepsilon}^{p(k)}_{n+1}) \leqslant 0$, then:

$$\mathbf{C}^{ep} = \mathbf{\Xi}_{n+1} + r^{-1} \mathbf{T}_{n+1} \otimes \mathbf{S}_{n+1}$$
$$\bar{\varepsilon}^p_{n+1} = \bar{\varepsilon}^{p(k)}_{n+1}$$
$$\boldsymbol{\sigma}_{n+1} = \boldsymbol{\sigma}^{(k)}_{n+1}, \text{ Exit}$$

Endif

7. Calculate the incremental consistency parameter

$$\mathbf{r}_\circ = \boldsymbol{\sigma}_{n+1}^{(k)} - \left(\boldsymbol{\sigma}_n - \lambda_{n+1}^{(k)}\mathbf{C} : \frac{\partial f(\boldsymbol{\sigma}_{n+1}^{(k)}, \mathbf{Q}_{n+1}^{(k)})}{\partial \boldsymbol{\sigma}}\right)$$

$$\mathbf{M} = \mathbf{I} + \lambda_{n+1}^{(k)}\mathbf{C} : \frac{\partial}{\partial \boldsymbol{\sigma}}\left(\frac{\partial f(\boldsymbol{\sigma}_{n+1}^{k}, \mathbf{Q}_{n+1}^{(k)})}{\partial \boldsymbol{\sigma}}\right)$$

$$\Delta\lambda_{n+1}^{(k)} = \frac{f_\circ - \frac{\partial f}{\partial \boldsymbol{\sigma}}\Big|_{n+1}^{(k)} : \mathbf{M}^{-1}\mathbf{r}_\circ}{\frac{\partial f}{\partial \boldsymbol{\sigma}}\Big|_{n+1}^{(k)} : \mathbf{M}^{-1}\mathbf{C} : \frac{\partial f}{\partial \boldsymbol{\sigma}}\Big|_{n+1}^{(k)} + \frac{\partial f}{\partial \boldsymbol{\sigma}}\Big|_{n+1}^{(k)} : \mathbf{M}^{-1}\left(\lambda_{n+1}^{(k)}\mathbf{C} : \frac{\partial}{\partial \mathbf{Q}}\left(\frac{\partial f}{\partial \boldsymbol{\sigma}}\right)\Big|_{n+1}^{(k)}\frac{\partial \mathbf{Q}}{\partial \bar{\varepsilon}^p}\Big|_{n+1}^{(k)} + \frac{\partial f}{\partial \mathbf{Q}}\Big|_{n+1^{(k)}}\frac{\partial \mathbf{Q}}{\partial \bar{\varepsilon}^p}\Big|_{n+1}^{(k)}\right) + \frac{\partial f}{\partial \boldsymbol{\sigma}}\Big|_{n+1}^{(k)} : \mathbf{M}^{-1}\frac{\partial f}{\partial \bar{\varepsilon}^p}\Big|_{n+1}^{(k)}}$$

$$\lambda_{n+1}^{(k+1)} = \lambda_{n+1}^{(k)} + \Delta\lambda_{n+1}^{(k)}$$

$$k \leftarrow k+1$$

8. Go to step 5.

6. Numerical verifications

To validate the proposed algorithm, it was implemented as a user material model (UMAT) into ABAQUS finite element code. A biaxial tension test was carried out on the niobium sheet, by means of applying hydrostatic fluid pressure to bulge the sheet, and its results were compared with finite element simulations. Fig. 11c shows one-half of the bulged niobium sheet with fracture occurring parallel to the rolling direction and away from the pole of the sheet. Two different forms of Hill's quadratic yield function were used in the finite element simulation; one with constant anisotropic coefficients and the other with anisotropic coefficients evolving with plastic strain. Figs. 11a and b show the contour of the thickness strain in the bulged sheet predicted with and without the anisotropy coefficients evolving with the plastic strain, respectively. As can be seen from Figs. 11a and b, the yield function with evolutionary coefficients predicts, similar to the actual bulged sheet (Fig. 11c), two regions with strain localization in the deformed part. On the other hand, the yield function with constant coefficients does not show any strain localization. Fig. 12 shows the hoop stress–strain curves obtained from the biaxial bulging of the niobium sheet and the finite element simulations. It can be seen from this figure that predicted stresses obtained using a yield function with constant coefficients overpredicts the experimental curve, while the one with evolved coefficients very accurately match the experimental stress–strain curve.

7. Some observations on the texture of niobium sheet

It is recognized that the planar variation of the r-value is due to the anisotropy and texture of the rolled sheet. It is clear from Fig. 13 that the high purity niobium sheet has four extremums up to 20% strain. This suggests that the niobium sheet will exhibit six ears in a standard cup-drawing test. Between 20% and 25% strain it shows only two extremums, which implies it will develop only two ears. Beyond 25% strain it shows 5 extremums, which implies it will develop eight ears in the cup-drawing test.

A higher variation of the r-value occurs at around 25° and 65° orientations, and this variation is almost the same at 0°, 45° and 90°. These behaviors, where extremums of the r-values at 0° and 90° are not the maximum values, are known as the specific planar anisotropy. The anisotropic variation of the r-value in different direction, compared to the rolling direction, is related to the intensity of different orientations in the material's texture (see Asensio et al., 2001). The study by Toth et al. (1990), Liu et al. (2002), Park et al. (1997), and Nesterova et al. (2001) show that the recrystallization and deformation texture of the high purity niobium is very similar to those in deep drawing quality steels (low carbon steels) and molybdenum. Texture measurements from through-thickness of the niobium sheets showed that the main texture components of superconducting niobium sheet are on the α, γ, and ε fibers as shown in Fig. 14.

Fig. 15 shows the ODF sections at $\varphi_2 = 45°$ for the undeformed niobium sheet and uniaxially deformed at 67.5° compared to the rolling direction. The 67.5° was selected because the larger variation of the r-value occurs in this direction. An ODF section at 45° contains all three α, γ, and ε fibers. ODFs show a strong γ

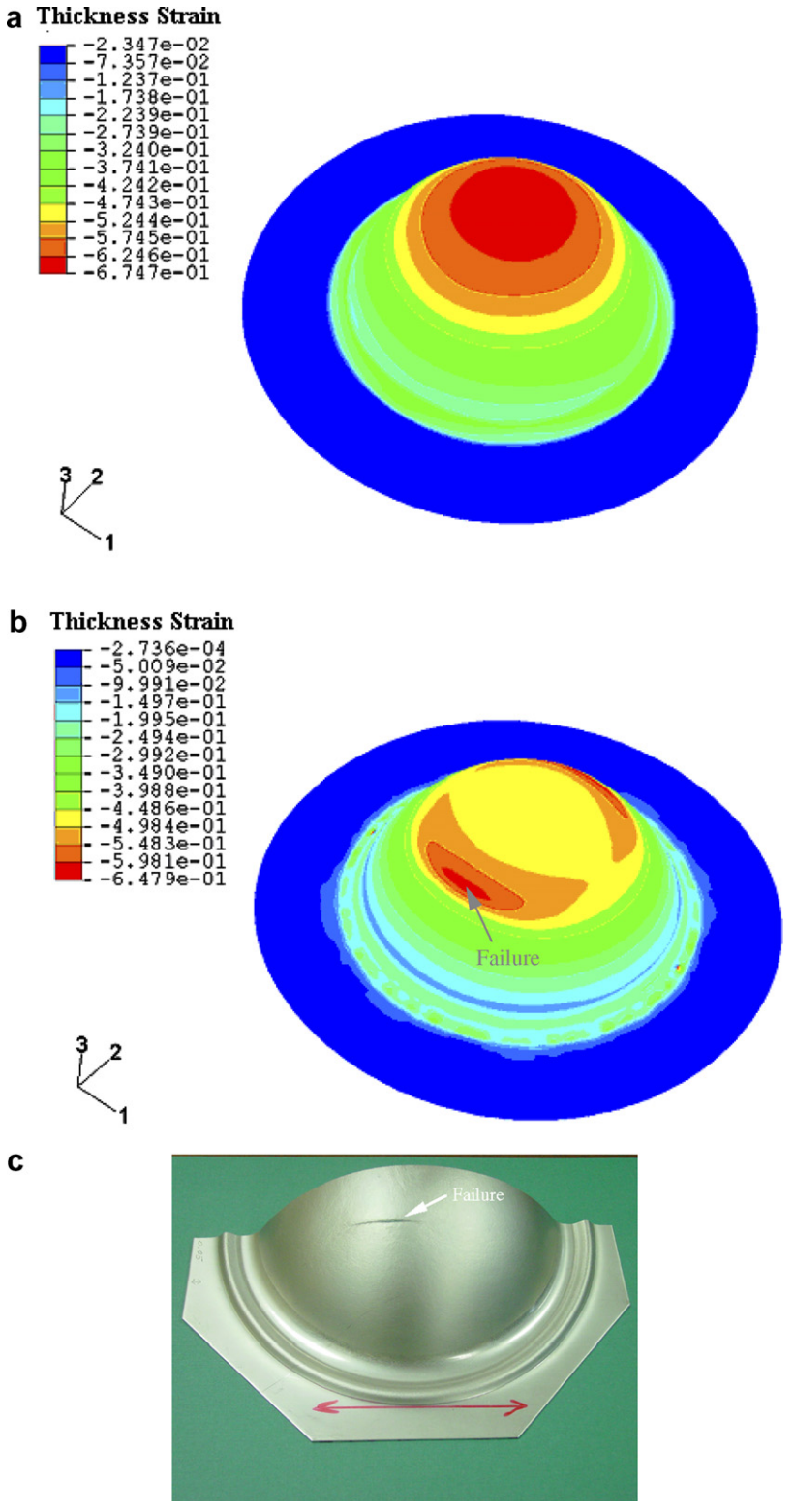

Fig. 11. (a) Simulation using yield function with constant coefficients. (b) Simulation using evolutionary yield function. (c) Experiment (half of bulged specimen) at strain rate $\dot{\varepsilon} = 0.05\ s^{-1}$.

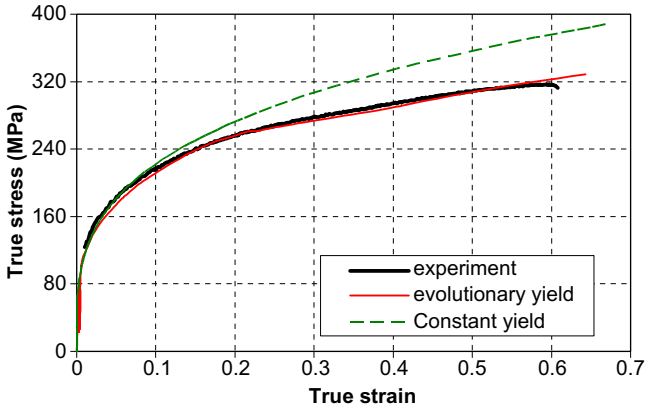

Fig. 12. Stress–strain curve for balanced biaxial bulge test obtained from experiment, simulation with constant yield function, and simulation with evolutionary yield function.

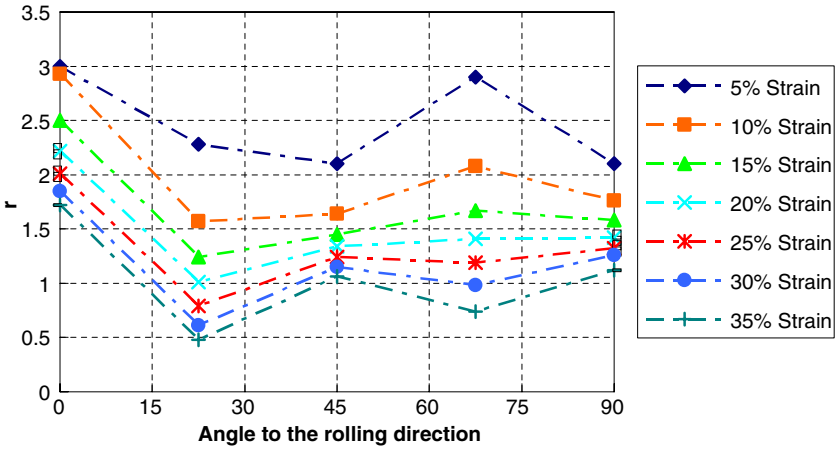

Fig. 13. Variation of the *r*-values with respect to the angle to the rolling direction and plastic strain.

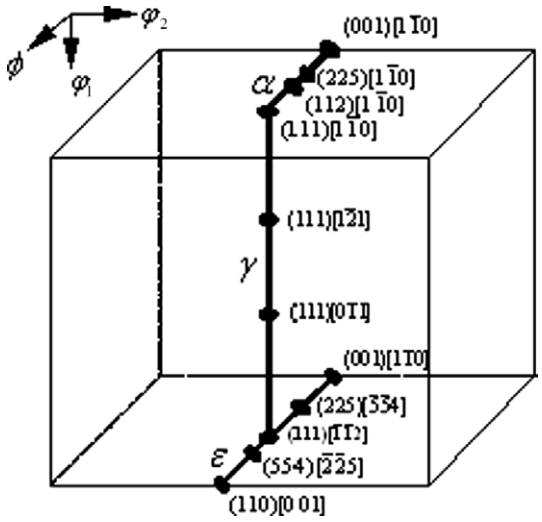

Fig. 14. Orientation distribution map for BCC materials.

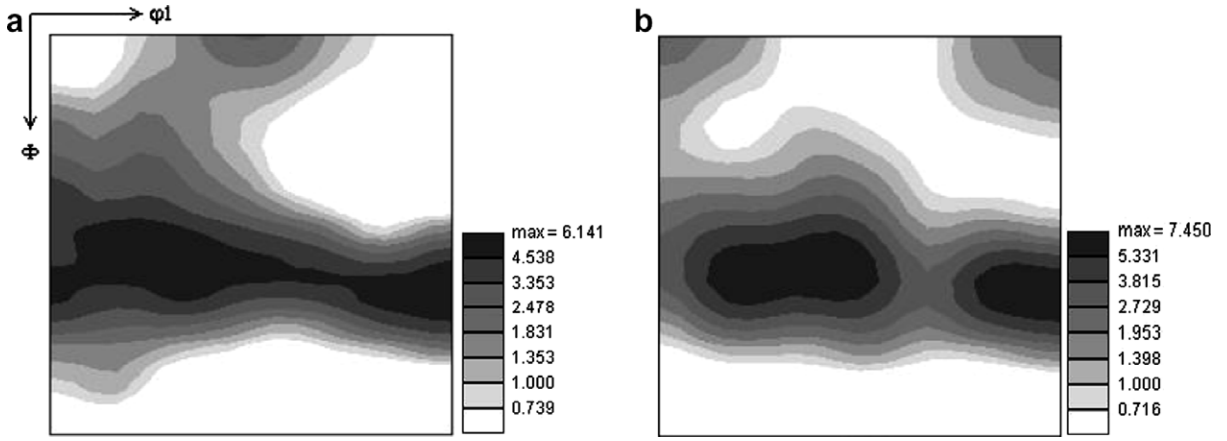

Fig. 15. ODF sections at $\varphi_2 = 45°$ for (a) undeformed superconducting niobium and (b) uniaxially deformed niobium.

fiber in both undeformed and uniaxially deformed niobium sheet. They also show intensity for some orientations along α fiber. Components of α fibers are different in undeformed and deformed case.

A more careful study of the ODFs shows some intensity for the cube orientation or $\{100\}\langle001\rangle$ in undeformed sheet and the rotated cube orientation or $\{100\}\langle011\rangle$ in deformed sheet. More information about the intensity of different components of texture in the α, γ, and ε fibers can be obtained by calculation of the skeleton diagrams for these fibers from ODFs as shown in Fig. 16. The skeleton diagram for γ fiber, Fig. 16a, shows an almost equal intensity of all orientations on γ fiber for the undeformed niobium, while it shows a lower intensity for $\{111\}\langle110\rangle$ and a maximum around $\{111\}\langle123\rangle$. On the average, intensity of γ fiber does not change with uniaxial deformation.

Fig. 16b shows the intensity of the different orientations on α fiber. The undeformed sheet shows a strong intensity for orientations from $\{112\}\langle110\rangle$ to $\{111\}\langle110\rangle$, while the deformed sheet shows a big drop in the intensity of the orientations around $\{112\}\langle110\rangle$ and $\{111\}\langle110\rangle$, and an increase of the rotated cube or $\{100\}\langle110\rangle$ orientations. The intensity of $\{100\}\langle110\rangle$ orientation in the deformed material is similar to $\{100\}\langle001\rangle$ in the undeformed sheet. Therefore, it seems that during deformation, the cube orientations in undeformed sheet convert to the rotated cube or $\{100\}\langle011\rangle$ orientations. The peak of intensity on α fiber in deformed sheet is around $\{554\}\langle110\rangle$.

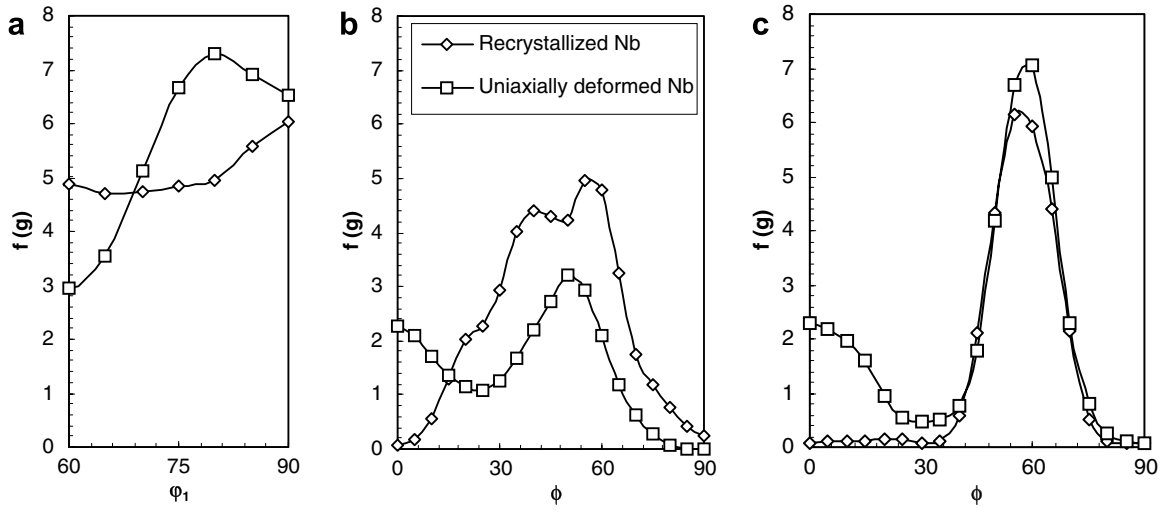

Fig. 16. Skeleton diagrams for superconducting niobium: (a) γ fiber, (b) α fiber and (c) ε fiber.

Fig. 16c shows the intensity of the orientations on ε fiber. The undeformed sheet shows intense orientations between $\{111\}\langle 112\rangle$ to $\{554\}\langle 225\rangle$. Uniaxial deformation cases increase on these orientations especially around $\{554\}\langle 225\rangle$. It has been observed that the $\{111\}\langle uvw\rangle$ or the γ fiber is not responsible for planar anisotropy, but other orientations like those between $\{112\}\langle 110\rangle$ to $\{111\}\langle 110\rangle$ in α fiber, $\{111\}\{112\}$ to $\{554\}\langle 225\rangle$ in ε fiber, and the cube $\{100\}\langle 001\rangle$ and rotated cube $\{100\}\langle 011\rangle$ orientations strongly affect the planar anisotropy. For low carbon BCC steels, usually intense orientations around $\{554\}\langle 225\rangle$ and the cube orientations or $\{100\}\langle 001\rangle$ show increase in r-value at 0° and 90°, and decrease in the r-value around 45°, while $\{112\}\langle 110\rangle$ to $\{111\}\langle 110\rangle$ orientations and the rotated cube or $\{100\}\langle 011\rangle$ have an inverse effect (see Vanderschueren et al., 2000).

There is no information about the effects of the above orientations on the planar anisotropy of the niobium sheet. The effects of different orientations on planar anisotropy are calculated with crystal plasticity models using a single crystal with different orientations. An example of such calculations can be found in the work of Daniel and Jonas (1990), which has been done for low carbon steel. Because of the important effect that planar anisotropy has on geometry, which is an important parameter in the design of superconducting niobium accelerator cavities, performing similar crystal plasticity calculations for the above orientations for the niobium sheet seems reasonable. This information will help in the texture design in the initial sheet or selecting suitable strain paths in the forming of superconducting niobium cavities.

8. Conclusions

In this work the formability and planar anisotropy of the high purity niobium sheet was investigated. Geometry is an important parameter in the design of superconducting accelerator cavities made with high purity niobium sheet. The following additional observations can also be made:

- The high purity niobium sheet shows a good formability due to a rather high $\bar{r}_m$ value, but it might not yield symmetric and uniform cavities with exact geometry due to the high $\Delta\bar{r}$ value during deep drawing process.
- The r-value of the high purity niobium sheet decreases with plastic strain.
- Applying a yield function with constant anisotropy coefficients cannot correctly predict the strain localization during the forming of the high purity niobium sheet.
- The r-values in different directions are representative of the microstructure and texture of a material and can be used to update the evolving anisotropy coefficients of the evolutionary yield function of the high purity niobium sheet as a function of the plastic strain.
- Usually $\Delta\bar{r}$ in BCC materials is constant during deformation and related to the difference between the r-values at 0°, 45°, and 90°. For the high purity niobium sheet, $\Delta\bar{r}$ is not constant and is more closely related to the variation of the r-values at around 25° and 65° during deformation.
- Texture of the undeformed niobium sheet contains an intense γ fiber, intense orientations between $\{112\}\langle 110\rangle$ to $\{111\}\langle 110\rangle$ on α fiber, and some intensity on cube orientation $\{100\}\langle 001\rangle$. After uniaxial deformation, the intensity of orientations around $\{111\}\langle 110\rangle$ in γ fiber decreases while the intensity of orientations around $\{111\}\langle 112\rangle$ increases. The α fiber of the uniaxially deformed niobium sheet shows a peak intensity around $\{554\}\langle 110\rangle$ and some intensity in the rotated cube or $\{100\}\langle 110\rangle$ orientation. Also, there are strong components in the vicinity of $\{554\}\langle 225\rangle$ orientations on the ε fiber of the deformed material.
- Reduction of the r-values with plastic strain might be related to the significant change in the components of the texture during the deformation of the niobium sheet. And the appearance of a high planar anisotropy in the niobium sheet can be related to the appearance of the strong components in $\{hkl\}\langle 110\rangle$ fiber of the niobium texture.

Acknowledgements

The authors wish to thank the National Science Foundation for the partial support of this project through the grant DMI 0084992 in conjunction with Alcoa through the GOALI program. Also, the partial support of this

project by the National Superconducting Cyclotron Lab (NSCL) at Michigan State University is greatly appreciated. Finally, the authors wish to thank Dr. John Carsley of General Motors for conducting the tensile tests.

References

ABAQUS manual, 2001. Hibbit, Karlsson & Sorensen Inc, Providence, RI, Version 6.3.

Asensio, J., Romano, G., Martnez, V.J., Verdeja, J.I., Pero-Sanz, J.A., 2001. Optimization of hot rolled textures through cold rolling and annealing. Mater. Characteriz. 47, 119.

Barlat, F., Lian, J., 1989. Plastic behavior and stretchability of sheet metals. Part I: Yield function fororthotropic sheets under plane stress conditions. Int. J. Plasticity 5, 51.

Barlat, F., Lege, D.J., Brem, J.C., 1991. A six-component yield function for anisotropic metals. Int. J. Plasticity 7, 693.

Barlat, F., Chung, K., Richmond, O., 1993. Strain rate potential for metals and its application to minimum plastic work path calculations. Int. J. Plasticity 9, 1.

Barlat, F., Maeda, Y., Chung, K., Yanagawa, M., Brem, J.C., Hayashida, Y., Lege, D.J., Matsui, K., Murtha, S.J., Hattori, S., Becker, R.C., Makosey, S., 1997. Yield function development for aluminumalloy sheet. J. Mech. Phys. Solids 45, 1727.

Barlat, F., Brem, J.C., Yoon, J.W., Chung, K., Dicke, R.E., Legea, D.J., Pourboghrat, F., Choif, S.H., Chuh, E., 2003. Plane stress yield function for aluminum alloy sheets—Part 1: Theory. Int. J. Plasticity 19, 1297.

Bassani, J.L., 1977. Yield characterization of metals with transversely isotropic plastic properties. Int. J. Mech. Sci. 19, 151.

Budianski, B., 1984. Anisotropic plasticity of plane-isotropic sheets. In: Dvork, G.J., Shield, R.T. (Eds.), Mechanics of Material Behavior. Elsevier, Amsterdam, The Netherlands.

Daniel, D., Jonas, J.J., 1990. Measurement and prediction of plastic anisotropic in deep drawing steels. Metall. Trans. A 21A, 331.

Gotoh, M., 1977. A theory of plastic anisotropy based on a yield function of fourth order (plane stress state). Int. J. Mech. Sci. 19, 505.

Hershey, A.V., 1954. The plasticity of an isotropic aggregate of anisotropic face centered cubic crystals. J. Appl. Mech. 30, 241.

Hill, R., 1948. A theory of the yielding and plastic flow of anisotropic metals. Proc. R. Soc. London. Ser. A Math. Phys. Sci. 193 (1033), 281.

Hill, R., 1979. Theoretical plasticity of textured aggregates. Math. Proc. Camb. Phil. Soc. 85, 179.

Hill, R., 1990. Constitutive modeling of anisotropic plasticity in sheet metals. J. Mech. Phys. Solids 38, 405.

Hosford, W.F., 1972. A generalized isotropic yield criterion. J. Appl. Mech. 39, 607.

Kneisel, P., Palmieri, V., 1999. Development of seamless niobium cavities for accelerator applications. In: Proceeding of the 1999 Particle Accelerator Conference, New York, 943.

Liu, Y.S., Delannay, L., Van Houtte, P., 2002. Application of the Lamel model for simulating cold rolling texture in molybdenum sheet. Acta Mater. 50, 1849–1856.

Logan, R., Hosford, W.F., 1980. On yield loci of anisotropic cubic metals. Int. J. Mech. Sci. 22, 419.

Nakamachi, E., Xie, C.L., 2003. Design of texture for improved formability of high-strength steel. Mater. Sci. Eng. A 340, 130.

Nemat-Nasser, S., Guo, W., 2000. Flow stress of commercially pure niobium over a broad range of temperatures and strain rates. Mater. Sci. Eng. A 284, 202.

Nesterova, E.V., Bacroix, B., Teodosiu, C., 2001. Experimental observation of microstructure evolution under strain-path changes in low-carbon IF steels. Mater. Sci. Eng. A 309, 495.

Pagani, C., Barni, D., Bosotti, A.,Pierini, P., 2001. Design critical for elliptical cavities. In: Proceeding of the 2001 Particle Accelerator Conference, Japan.

Palmieri, V., 1999. New technology in superconducting cavity fabrication. IEEE Trans. Apll. Supercond. 9 (2), 1036.

Park, Y.B., Lee, D.N., Gottstein, G., 1997. Evolution of recrystallisation texture from cold rolling textures in interstitial free steel. Mater. Sci. Technol. 3403, 289.

Piehler, H.R., 1967. Sc. D. thesis, Massachusett Institute of Technology, Cambridge.

Read-Hill, R.E., Kaufman, M.J., 1994. On evaluation the flow stress in niobium of commercial purity. Acta Matter. 43 (5), 1731.

Singer, W., Kaiser, H., Singer, X., Weichert, G., Jelesov, I., 2001. Hydroforming of superconducting tesla cavities. In: Proceeding of the 2001 Particle Accelerator Conference, Japan.

Singer, W., Kaiser, H., Singer, X., Weichert, G., Jelesov, I., Khabibuline T., 2001. Hydroforming of NBCU clad cavities at DESY. In: Proceeding of the 2001 Particle Accelerator Conference, Japan.

Toth, L.S., Jonas, J.J., Daniel, D., Ray, R.K., 1990. Development of Ferrite rolling textures in low carbon steels. Metall. Trans. 21A, 2985.

Vanderschueren, D., Yoshinaga, N., Kestens, L., 2000. Texture and anisotropy control of IF high strength steel. In: IF steel Conference 2000, Pittsburgh, p. 247.

Yoon, J.W., Barlat, F., Dick, R.E., Chung, K., Kang, T.J., 2003. Plane stress yield function for aluminum alloy sheets – Part II: FE formulation and its implementation. Int. J. Plasticity 20, 495.

Zamiri, A., Pourboghrat, F., Jiang, H., Bieler, T.R., Barlat, F., Brem, J., Compton, C., Grimm, T.L., 2006. On mechanical properties of the superconducting niobium. Mater. Sci. Eng. A 435–436, 658–665.